HEFAT2014
10th International Conference on Heat Transfer, Fluid Mechanics and Thermodynamics
14 – 16 July 2014
Orlando, Florida

TWO-DIMENSIONAL TOPOLOGY OPTIMIZATION OF FLUID CHANNEL DISTRIBUTIONS – PRESSURE OBJECTIVE

Nel G., Dirker J*. and Meyer J.P.
*Author for correspondence
Department of Mechanical and Aeronautical Engineering,
University of Pretoria,
Pretoria, 0002,
South Africa,
E-mail: jaco.dirker@up.ac.za

ABSTRACT

In this two dimensional numerical study, miniature cooling channel lay-outs were obtained using topology optimization techniques. Laminar steady state flow was considered for different inlet and outlet configurations. A pressure minimization objective was considered in this paper. The physics of the primary system was controlled via a discreet design variable set and implemented in the model using the finite volume method. To improve convection effects, design level cells were sub-divided into up to three by three computational sub cells. It was found that improved material distributions with discrete solid-to-liquid interfaces were obtained when a global (domain wise) objective function was used and the placement of solid and liquid cells were done according to the gradient-based sensitivities of the objective functions. It was found that flow-rate-specific topology optimization was needed to reduce over-all pressure drop.

INTRODUCTION

As technology advances, increased demands are made on the output of modern electronics. Higher output requirements leads to increased power consumption for these devices, resulting either in increased operating temperatures or higher demands on the heat removal systems to sustain desired efficiency levels. When considering the cooling of these devices the amount of heat transferred is critical to the operating temperature. Heat transfer using pure conduction alone is insufficient for cooling higher heat generating density cases. By introducing flow channels into a heat producing domain the heat transfer can be significantly increased through convection heat transfer but at the increased cost of pumping the fluid. Heat flux levels sustained with convection are orders larger than the heat flux levels that can be supported by conduction only. For this reason combined fluid-solid systems require further investigation. In this paper only the minimization of pressure across the flow channels will be considered and forms the first part of understanding the contradicting objective of high heat transfer and low pressure

NOMENCLATURE

C, C_s, C_f	[Pa]	Pressure coefficients
F	m^2/s.	Body force
j		Objective function
J		Integrated objective function
L		Lagrangian function
m	[-]	Design variable
N	[-]	Number of design cells
p	$[m^2/s^2]$	Kinematic pressure of the fluid
P	[Pa]	Pressure of fluid
Q		Residual stat variable
r_a	[-]	Number of cells added
r_r	[-]	Number of cells removed
R		Residual stat variable
R_a	[-]	Addition rate
R_r	[-]	Removal rate
Re	[-]	Reynolds Number
t	[-]	Iteration step number
u, U	[m/s]	Velocity of the fluid
V_f	[-]	Volume fraction
x	[m]	Cartesian axis direction
y	[m]	Cartesian axis direction
z	[m]	Cartesian axis direction
Special characters		
α	$[m^2/s]$	Thermal diffusivity
$\mathcal{T}$	[-]	Domain boundary
λ	[-]	Adjoint velocity
$\varnothing$	[-]	Adjoint pressure
τ	[m]	Permeability
γ	[-]	Ratio between thermal diffusivities of cooling fluid and the heat-generating solid
Ω	[-]	Domain
Subscripts		
i		Design cell index
I		Inlet
j		In terms of j
l		Liquid phase
O		Outlet
p		In terms of p
s		Solid phase
W		Wall
Superscripts		
n		Normal component
t		Tangential component

drops. In general, the aim would be to find the best layout for the flow channels that meet the requirements in the limited sized domain. The necessity to increase the performance of such systems warrants the use of optimization techniques such as topology optimization which sole goal is to obtain advantageous internal layouts.

Topology optimization is a wide field with applications in among others, structural systems [1] and fluid systems [2-4]. Early pioneering work in topology optimization was presented by Bendsoøe in his paper on homogenization [5]. His work was further extended to other methods [6, 7] in the structural optimization and thermal conduction [8]. Application on combined thermal-flow systems was also investigated by [9].

In topology optimization there are two types of methods that are generally used for the optimization: gradient based and gradient free method. Gradient based methods require a sensitivity analysis to determine the gradients of the objective function. Such sensitivities are used in optimization algorithms to control the adjustment of the topology. Gradient free methods only require the availability of the objective. Both genetic and evolutionary type methods all fall under gradient free methods and rely on logic to control the topology. A gradient based method was used in this paper to increase the convergence rate of the optimization.

Computation of gradients can be done using direct or indirect methods using analytical or numerical methods. Finite difference is a good example of a common direct, numerical method and is widely used to determine gradients. Direct methods are used for systems with many objective functions and a few parameters, and indirect methods are used for systems with large number of parameters and a few objective functions. The adjoint method is considered an indirect method and is of particular interest for topology optimization due to the large number of parameters present. Computational costs play a significant role in the selection of the methods used and the computational costs for adjoint methods are independent of the number of parameters. The computational costs for direct methods scale non-linearly with the number of parameters. This is the primary reason why adjoint methods are well suited to topology optimization problems.

Two formulations for adjoint methods exist, continuous and discrete. In continuous adjoint method the governing partial derivative equations (PDE's) are differentiated in terms of the parameters, to derive the adjoint equations and boundary conditions, and are then discretised. In discrete adjoint methods the governing PDE's are first discretised and then differentiated in terms of the parameters to obtain the adjoint equations. The accuracy of adjoint sensitivities will later be compared to finite difference gradients. A good review on the accuracies of the different approaches is discussed in [10, 11]. In this paper the continuous adjoint method was used to compute the gradients.

MODEL FORMULATION

The square two-dimensional computational domain used in this study is shown in Figure 1. In this configuration there is an inlet on the left hand boundary and two outlets on the right band boundary, each with a parabolic velocity profile as shown.

All other boundaries are taken as being adiabatic. The domain is divided into design cells. In this paper a design cell density of 50 by 50 was used, resulting in $N = 2500$ design cells. For clarity, a reduced number of design cells are shown in Figure 1. Each design cell can be toggled between a solid-state and liquid-state by changing its design variable m_i where i refers to the design cell number.

A discrete algorithm was used for the topology optimization to produce a discreet solution. Each design variable (m_i also called the fluid fraction in this application) assumed a value of either $m_i = 0$ for fluids or $m_i = 1$ for solids.

Each design cell was further divided into smaller sub cells, as shown in Figure 2, which were used to refine design cells and increase the accuracy of the sensitivities and the numerical flow solution, especially the convection effect. The finer resolution from the sub-cells allows better representation of the physics and the gradients in a cell. In this paper 1x1, 2x2 and 3x3 sub-divisions were used resulting in 2 500, 10 000 and 22 500 computational cells.

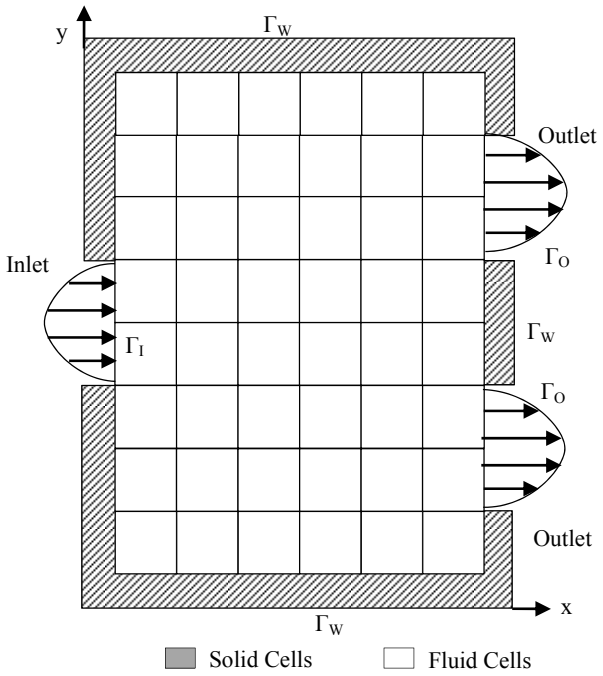

Figure 1 Design domain for a single inlet outlet system

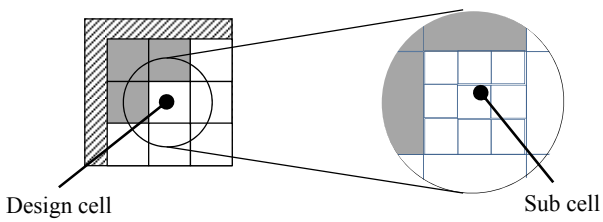

Figure 2 Division of design cell into smaller sub cells

Flow model

The flow in the domain, Ω, was modelled using the steady state, incompressible Navier-Stoke equations and the continuity equations:

$$\frac{\partial u_i}{\partial x_i} = 0 \quad in\ \Omega \tag{1}$$

$$u_j \frac{\partial u_i}{\partial x_j} = -\frac{\partial p}{\partial x_i} + \frac{\partial}{\partial x_i}(\nu \frac{\partial u_i}{\partial x_j} + \nu \frac{\partial u_j}{\partial x_i}) + \mathrm{F}_j \quad in\ \Omega \tag{2}$$

where u_i is fluid velocity, p is the fluid pressure, ν is fluid kinematic viscosity and F is the body force exerted on the fluid.

The governing equations were required to model both solid and liquids by changing the design variable, m_i. The continuity equation holds for both solid and liquids and only the Navier-Stokes equation needs modification depending on whether the material is solid or liquid. To model zero velocity in solid cells a porous friction term was introduced [9,10] as the body force term. The friction is dependent on the impermeability, τ, of the medium as well as the fluid velocity:

$$F_i = -\tau u_i \tag{3}$$

A dependence of the impermeability on the local fluid fraction, m_i, is used to control the velocity in each cell. For this purpose a linear material interpolation was used:

$$\tau(\mathrm{m}_i) = \tau_l + m_i(\tau_l - \tau_s) \tag{4}$$

where τ_l and τ_s are the liquid and solid impermeability respectively. A simple material interpolation model suffices since a discrete optimization approach was used and did not influence the physics. For approaches that use continuous design variable values, other interpolation schemes should be used. Since $m_i = 0$ presents a liquid cell τ_l was chosen as 0 to cancel out the friction term. For solids when $m_i = 1$, a large value was chosen for the permeability to approximate the solid. A solid permeability of $\tau_s = 300$ produce negligible velocity in solid cells ($u \sim 10^{-12}$). The final form of the flow governing equations is:

$$\frac{\partial u_i}{\partial x_i} = 0 \quad in\ \Omega \tag{5}$$

$$u_j \frac{\partial u_i}{\partial x_j} + \frac{\partial p}{\partial x_i} - \frac{\partial}{\partial x_i}(\nu \frac{\partial u_i}{\partial x_j} + \nu \frac{\partial u_j}{\partial x_i}) + \tau u = 0 \quad in\ \Omega \tag{6}$$

Commonly used boundary conditions for incompressible, steady flow are of the Dirichlet and Neumann types. The velocity boundary conditions on the edge of the domain, Γ, were selected as follows (refer to Figure 1):

$$u_i = U_i \quad on\ \Gamma_I \tag{7}$$

$$u_i = 0 \quad on\ \Gamma_W \tag{8}$$

$$\frac{\partial u_i}{\partial x_j} n_j = 0 \quad on\ \Gamma_O \tag{9}$$

where U_i is the specified inlet velocity and n_j the outward unit normal on Γ. While the following pressure boundary conditions were used:

$$\frac{\partial p}{\partial x_j} n_j = 0 \quad on \Gamma_I \tag{10}$$

$$\frac{\partial p}{\partial x_j} n_j = 0 \quad on \Gamma_W \tag{11}$$

$$p = 0 \quad on \Gamma_O \tag{12}$$

A non-slip boundary type was used for all domain edges associated with walls. Zero normal pressure and velocity gradients were used at the outlet.

Model Validation

The numerical model was validated using flow over a flat plate, amongst others, by using analytical results from the Blasius similarity solution. In Figure 3 the velocity profiles u are compared and are in good agreement with the analytical solution along the length scale η.

OPTIMIZATION

Optimization Statement

The topology optimization problem was implemented using a hybrid-based iterative method. The method was discrete and required the gradient of the objective function in order to determine the sensitivity of each cell in the domain. The discrete topology optimization for a general objective function, j, can be stated as:

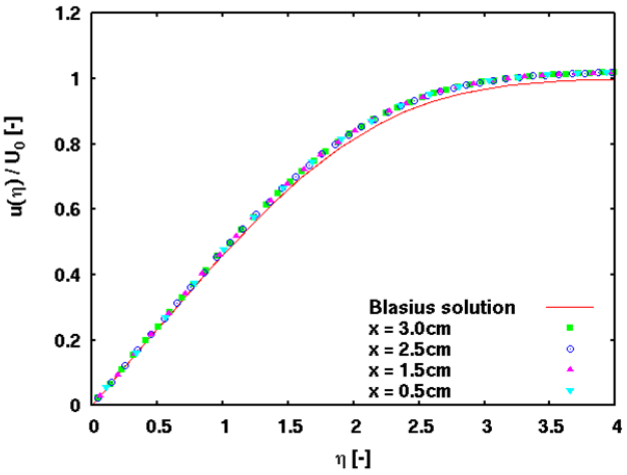

Figure 3 Validation using Blasuis flat plate solution

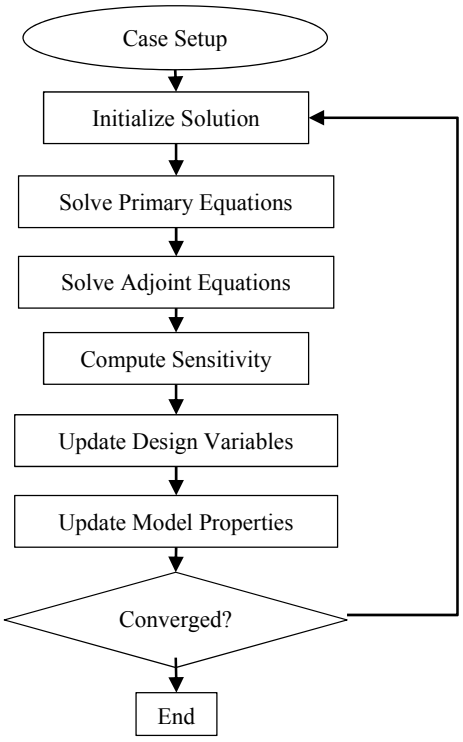

Figure 4 Flowchart of optimization algorithm

$$\begin{aligned} &\text{minimize } j(u_i, p, m) \\ &\text{such that } \int_\Omega m\, d\Omega \le V_f \quad m \in \{0,1\} \end{aligned} \tag{13}$$

An overview of the optimization algorithm is given in Figure 4. Initially the layout was chosen to be all liquid cells and solid cells were gradually added and removed from the layout. The rate at which solid was added r_a and removed r_r determined the convergence rate of the optimization algorithm.

Sensitivity analysis

The adjoint method [12] was used to determine the sensitivities of the objective function. For this purpose the optimization problem need to be transformed into an unconstrained problem using the Lagrangian method. The extended objective function is:

$$L = J + \int_\Omega (\lambda_i \mathrm{R}_i + \phi \mathrm{Q})\, d\Omega \tag{14}$$

The adjoint velocity, λ_1 and adjoint pressure, ϕ, are the Lagrange multipliers. Given that the governing equations are satisfied, $R_i = Q = 0$, they will act as equality constraints for the optimization. The first variation of the extended objective function in Eqn. (14) is:

$$\delta L = \delta J + \int_\Omega \lambda_i\, \delta \mathrm{R}_i\, d\Omega + \int_\Omega \phi\, \delta \mathrm{Q}\, d\Omega \tag{15}$$

The variation of the objective function can be separated into the contribution from the boundary and the contribution from the domain:

$$\delta J = \int \delta j_\Gamma\, d\Gamma + \int \delta j_\Omega\, d\Omega \tag{16}$$

The variation of the extended objective function is:

$$\delta L = \delta_m L + \delta_{u_i} L + \delta_p L \tag{17}$$

The above variation includes contribution from the state variables (u, p) and the local design variable (m_i). Computing the sensitivities from Eqn. (17) directly would require the solution of the governing equation for each design variable which would be problematic due to computational restrictions. To address this problem, the adjoint variables can be chosen in such a way that their variation is zero with regard to the state variables:

$$\delta_{u_i} L + \delta_p L = 0 \tag{18}$$

Variations of the governing equations can be written to be:

$$\begin{aligned} \delta_u R_i &= \delta u_j \frac{\partial u_i}{\partial x_j} + u_j \frac{\partial \delta u_i}{\partial x_j} - \frac{\partial}{\partial x_j}\left(\nu \frac{\partial \delta u_i}{\partial x_j} + \nu \frac{\partial \delta u_j}{\partial x_i}\right) + \tau \delta \mathrm{u}_i \\ \delta_u Q &= -\frac{\partial \delta u_j}{\partial x_i} \end{aligned} \tag{19}$$

$$\begin{aligned} \delta_p R_i &= \frac{\partial \delta p}{\partial x_i} \\ \delta_p Q &= 0 \end{aligned} \tag{20}$$

Combining the variation yields:

$$\begin{aligned} \delta L = &\int \delta j_\Gamma\, d\Gamma + \int \delta j_\Omega\, d\Omega \\ &\int_\Omega \lambda_i \left(\delta u_j \frac{\partial u_i}{\partial x_j} + u_j \frac{\partial \delta u_i}{\partial x_j} - \frac{\partial}{\partial x_j}\left(\nu \frac{\partial \delta u_i}{\partial x_j} + \nu \frac{\partial \delta u_j}{\partial x_i}\right) + \tau \delta \mathrm{u}_i + \frac{\partial \delta p}{\partial x_i}\right) d\Omega \\ &\int_\Omega \phi \left(-\frac{\partial \delta u_j}{\partial x_i}\right) d\Omega \end{aligned} \tag{21}$$

The basic method of adjoint sensitivity analysis is to choose the adjoint variables in such a way that their contribution to sensitivity is eliminated. In order to eliminate gradients of variation they are integrated and grouped.

$$\begin{aligned} &\int_\Omega \left(-u_j \frac{\partial \lambda_j}{\partial x_i} \delta u_i - u_j \frac{\partial \lambda_i}{\partial x_j} \delta u_i + \tau \lambda_i \delta u_i - \frac{\partial}{\partial x_j}\left(\nu \frac{\partial \lambda_i}{\partial x_j} + \nu \frac{\partial \lambda_j}{\partial x_i}\right) \delta u_i - \frac{\partial \lambda_i}{\partial x_i} \delta p\right) d\Omega \\ &+ \int_\Gamma \left(\lambda_j n_i u_j \delta u_i + u_j n_j \lambda_i \delta u_i + \lambda_j n_j \delta p + \nu n_j \left(\frac{\partial \lambda_i}{\partial x_j} + \frac{\partial \lambda_j}{\partial x_i}\right) \delta u_i - \nu \lambda_i n_j \left(\frac{\partial \delta u_i}{\partial x_j} + \frac{\partial \delta u_j}{\partial x_i}\right)\right) d\Gamma \\ &+ \int_\Omega \left(\delta u_i \frac{\partial \phi}{\partial x_i}\right) d\Omega + \int_\Gamma \left(-\phi n_i \delta u_i\right) d\Gamma \end{aligned} \tag{22}$$

The adjoint equations are derived from the volume integrals and must be satisfied on the entire domain. By combining terms and rearranging, the adjoint equations become:

$$-u_j \frac{\partial \lambda_j}{\partial x_i} - u_j \frac{\partial \lambda_i}{\partial x_j} + \tau \lambda_i - \frac{\partial}{\partial x_i}(\nu \frac{\partial \lambda_i}{\partial x_j} + \frac{\partial \lambda_j}{\partial x_i}) + \frac{\partial \phi}{\partial x_i} + \frac{\partial j_\Omega}{\partial u_i} = 0 \quad (23)$$

$$\frac{\partial \lambda_j}{\partial x_j} = \frac{\partial j_\Omega}{\partial p} \quad (24)$$

Boundary conditions arise from the extra boundary integral terms, and are chosen to vanish such that these have no influence on the sensitivity calculations.

$$(\lambda_j n_i u_j + u_j n_j \lambda_i + \nu n_j \frac{\partial \lambda_i}{\partial x_j} - \phi n_i + \frac{\partial j_\Gamma}{\partial u_i})\delta u_i - (\nu \mathrm{n}_j \lambda_i)\frac{\partial \delta u_i}{\partial x_j} \quad (25)$$

$$(\lambda_i n_i + \frac{\partial j_\Gamma}{\partial p})\delta p \quad (26)$$

In this study the adjoint boundary conditions were chosen as follows:

For the adjoint velocity:

$$\lambda_i n_i = -\frac{\partial j_\Gamma}{\partial p} \quad on \quad \Gamma_I \quad (27)$$

$$\lambda_i = 0 \quad on \quad \Gamma_W \quad (28)$$

$$u^n \lambda_i^T + \nu n_j \frac{\partial u_i^T}{\partial \mathrm{x}_\mathrm{j}} + \frac{\partial j_\Gamma}{\partial u_i^T} = 0 \quad on \quad \Gamma_O \quad (29)$$

For the adjoint pressure:

$$\frac{\partial \phi}{\partial x_i} n_i = 0 \quad on \quad \Gamma_I \quad (30)$$

$$\frac{\partial \phi}{\partial x_i} n_i = 0 \quad on \quad \Gamma_W \quad (31)$$

$$\phi = \lambda_j u_j + u^n \lambda^n + \nu n_j \frac{\partial \mathrm{u}^\mathrm{n}}{\partial \mathrm{x}_\mathrm{j}} + \frac{\partial j_\Gamma}{\partial u^n} \quad on \quad \Gamma_O \quad (32)$$

The objective function sensitivity is only dependent on the design variable m_i:

$$\delta L = \delta_{m_i} L + \int_\Omega (\lambda_i \delta_{m_i} \mathrm{R}_i + \phi \delta_{mi} Q) d\Omega \quad (33)$$

It can thus be computed directly from:

$$\frac{dL}{dm_i} = \frac{\partial J}{\partial m_i} + \int_\Omega (\lambda_j \frac{\partial \mathrm{R}_j}{\partial m_i} + \phi \frac{\partial Q}{\partial m_i}) d\Omega \quad (34)$$

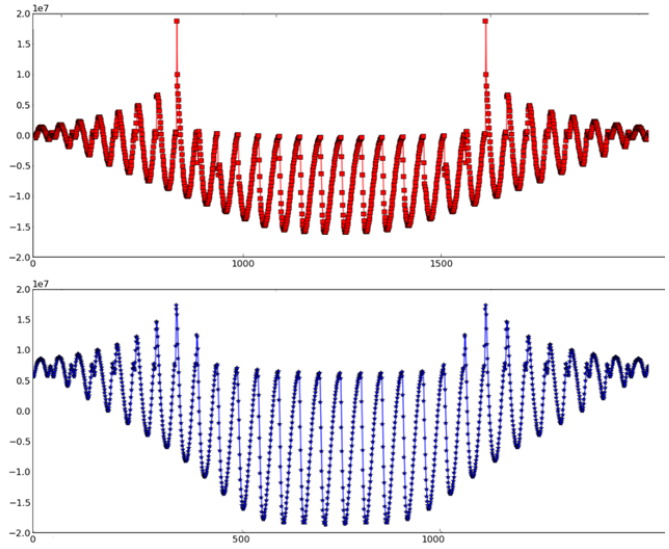

Figure 5 Finite Difference vs Adjoint sensitivities

The only dependence on the design variable is the impermeability for the flow model resulting in:

$$\frac{dL}{dm_i} = \frac{\partial J}{\partial m_i} + \int_\Omega (\lambda_j \frac{\partial \tau}{\partial m_i}) d\Omega \quad (35)$$

Adjoint Sensitivity Validation

The sensitivities obtained by the adjoint method were compared with the sensitivities computed using the direct finite difference method for a pressure objective function. Figure 5 gives the adjoint sensitivities on the top and the sensitivities according to the direct method on the bottom for the 2 500 design cells. It can be seen that there is a good agreement between the methods. The differences that do exist are due to the use of first order schemes and boundary approximations that were implemented. Based on the good agreement, the adjoint sensitivities were used in this study.

RESULTS

In this section several applications of the model and optimization will be demonstrated. The optimal layout of flow channels for the pressure drop objective will be demonstrated. The effect of the design cells on the optimization is also presented, specifically the cell refinement and the addition and removal rate of solid material.

The topology optimization was applied to the two dimensional layout as depicted in Figure 6. The layout is a simple double inlet - single outlet system where flow enters from the left and bottom and exits at the right. Both inlets had the same width. The domain was divided into 50 by 50 design cells with a 3 by 3 cell refinement for a total of 22 500 elements. To indicate the influence of the sub-cell refinement, the domain size was fixed for each case and the cell refinement was varied.

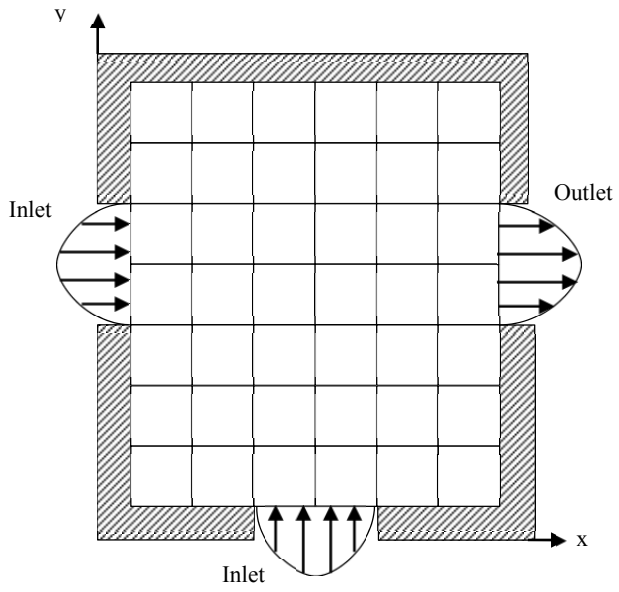

Figure 6 Simplified computational domain for demonstration purposes

The initial configuration for all cases was that the entire domain was liquid, $m = 0$. Cells with high sensitivity were toggled to solids until the volume constraint was met.

Figure 7 shows the progression of the optimization process for an inlet Reynolds number of $Re = 400$, an addition rate of $R_a = 0.0032$ (8 cells) and a removal rate of $R_r = 0.0016$ (4 cells) for the two inlet one outlet, layout as shown in Figure 4. The normalized addition, R_a, and removal rates, R_r, are defined as:

$$R_a = \frac{r_a}{N} \qquad R_r = \frac{r_r}{N} \tag{36}$$

Where r_a, r_r, and N are the addition rate, removal rate and the total number of design cells respectively.

The characteristic length used in the Reynolds number was the width of the two inlets. Iteration steps $t = 100$, $t = 200$, $t = 300$ and $t = 400$ are given which represent solid volume proportion of $V_f = 0.2$, 0.4, 0.6 and 0.8. The pressure and velocity contours are shown side by side for comparison. The solid domain is filled black and the contours of velocity and pressured displayed in the fluid region. From the solutions it can be seen that the most inefficient material is removed first, specifically the material in corners and near stagnation zones. By the 100th time step feint traces of the topology were already becoming visible. As the optimization iterations progressed more of the cells that contained slow flowing liquid were toggled to solids, until a well-defined topology was visible at a global solid volume ratio of 0.8 at $t = 400$.

The other flow branches sizes were then reduced until they are removed to produce a continuous branchless topology. Recirculation zones are responsible for the existence of the branches and increases with the flow velocity.

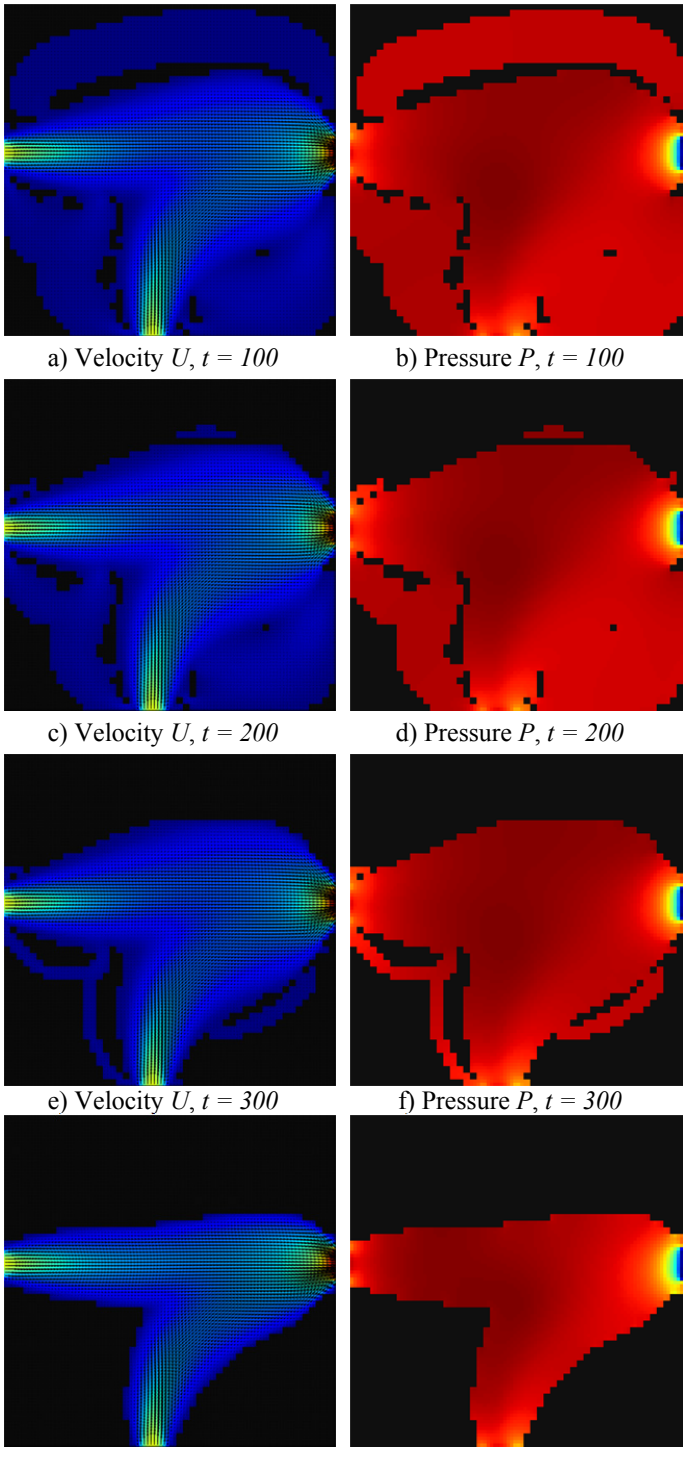

a) Velocity U, $t = 100$ b) Pressure P, $t = 100$

c) Velocity U, $t = 200$ d) Pressure P, $t = 200$

e) Velocity U, $t = 300$ f) Pressure P, $t = 300$

g) Velocity U, $t = 400$ h) Pressure P, $t = 400$

Figure 7 Optimization process at different steps

Design Cell Refinement

Cell level refinement was used to increase the accuracy of the convection physics in single cell channels. This also has the added effect of increasing the stability of the convergence. The effect of the design cell refinement on the optimization was

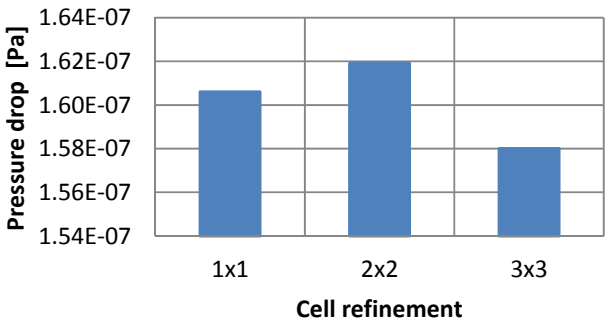

Figure 8 Pressure drop comparison for cell refinement

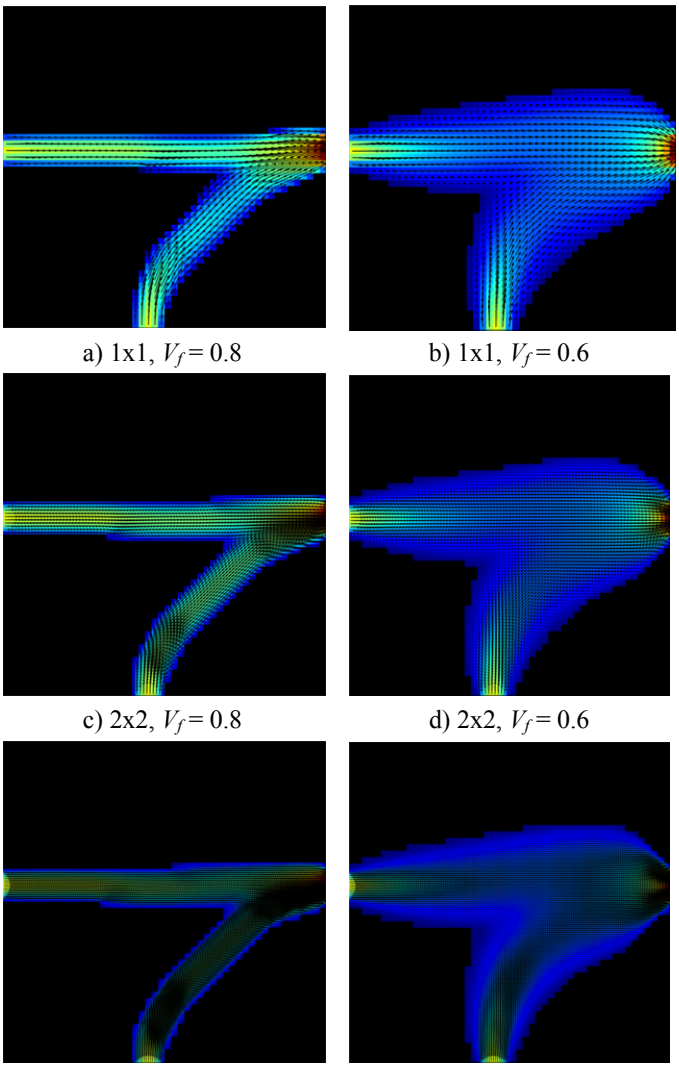

a) 1x1, $V_f = 0.8$ b) 1x1, $V_f = 0.6$

c) 2x2, $V_f = 0.8$ d) 2x2, $V_f = 0.6$

e) 3x3, $V_f = 0.8$ f) 3x3, $V_f = 0.6$

Figure 9 Cell refinement results

once again investigated for a configuration with two inlets and one outlet. Flow enters through the inlet on the left and bottom of the domain and exits at the right as shown in Figure 6.Varying refinement levels of 1x1, 2x2 and 3x3 were considered. An inlet Reynolds number of $Re = 400$ was used. The pressure drops for the three cell refinement levels are given in Figure 8 after $t = 400$. It can be obtain that the largest variation in the objective function for this example was only 2.5% when the sub cells were refined from 2x2 to 3x3. Figure 9 shows the optimization results for the flow channel using different cell refinements (1x1, 2x2 and 3x3) at two different global solid volume proportions ($V_f = 0.6$ after $t = 300$ and $V_f = 0.8$ after $t = 400$). Small differences in the solution can be seen for the final results of three different refinement levels.

The largest difference occurs where the two flows combine. For the pressure based objective function a sub cell refinement above 3x3 does not produce significant improvement in accuracy. This is because converged solutions of this type generally have wide flow channels allowing for relatively sufficient computation cells for the velocity field to be represented. Further refinement becomes too computationally expensive to perform without a suitable return on accuracy improvement. Higher design cell refinement is best suited for cases where the resulting flow channels in the topology are narrow such as when a flow channel is only one or two design cells wide, such as when a temperature based objective function is used (not covered in this paper).

Addition and removal rate

The addition and removal rate is an indication of the convergence rate of the optimization process. High addition rates may steer the solution away from the optimal or may even not converge altogether. It is important to study the effect of the addition and removal rate on the final solution.

For the addition and removal rate study the design domain depicted in Figure 6 was used again, but only for a 2x2 cell refinement. The inlet Reynolds number was again fixed at $Re = 400$ and a volume fraction of $V_f = 0.6$ was considered. Four addition rate and removal rate combinations are presented here: $R_a = 0.0032$ with $R_r = 0.0016$ which resulted in a net solid cell increase of 4 cells per iteration, $R_a = 0.0064$ with $R_r = 0.0032$ resulting in a net increase of 8 cells per iteration, $R_a = 0.0128$ with $R_r = 0.0032$ resulting in a net increase of 24 cells and $R_a = 0.0128$ with $R_r = 0.0064$ resulting in a net increase of 16 cells per iteration.

The results of the additional-removal study are shown in Figure 10. It can be seen that for this example the addition and removal rates had a small effect on the final topology. In general lower rates allow for finer resolution of the final rate but at the cost of making the optimization process slower.

Application - Pressure

The topology optimization will now be applied to the two dimensional layout as depicted in Figure 1. The layout is a simple single inlet and double outlet system where flow enters from the left and exits on the right and can be viewed as a simplified manifold. As before, the domain was divided into 50x50 design cells with a 3x3 cell refinement. The objective function can be represented as:

$$\begin{aligned} &\text{minimize } \mathrm{j}(u_i, p, m) = \int_\Gamma (P_I - P_O) \\ &\text{such that } \int_\Omega m\, d\Omega \le V_f \quad m \in \{0,1\} \end{aligned} \tag{37}$$

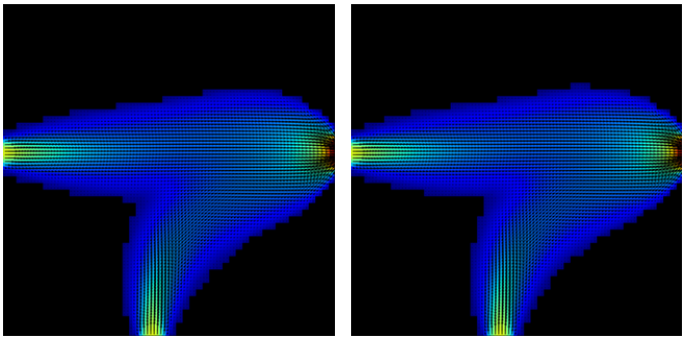

a) $R_a = 0.0032$, $R_r = 0.0016$ b) $R_a = 0.0064$, $R_r = 0.0032$

c) $R_a = 0.0128$, $R_r = 0.0032$ d) $R_a = 0.0128$, $R_r = 0.0064$

Figure 10 Influence of the addition and removal rate

The problem was analysed for different inlet Reynolds numbers, $Re = 50$, $Re = 100$, $Re = 400$ and $Re = 700$, at different volume fractions, $V_f = 0.6$ and $V_f = 0.8$.

A collection of optimized flow channel distributions for the pressure-based objective is shown in Figure 11.At first glance the increase in Reynolds number from $Re = 50$ to $Re = 100$ does not have a large impact on the final solution when compared to the $Re = 400$ and $Re = 700$ results. The increase in Reynolds number changes the lay-out from a Y-type shape towards a T-type shape, effectively decreasing the lengths of the channel branches to the outlets. By comparing the $V_f = 0.6$ cases with the $V_f = 0.8$ cases it could be seen that the higher velocities (red in colour) present when the channels were wider, formed clearly defined jet-like streams indicative of the possible lay-outs of the final narrower channels. It may also be noted that the solutions obtained were symmetric.

In Figure 12 the pressure drop ($P_I - P_O$) for the optimised layouts obtained with a single inlet, double outlet arrangement at different Reynolds numbers are shown for $V_f = 0.8$. To show the importance of the Reynolds-number-specific topology optimization, where each Reynolds number case had a different optimized topology, the pressured drop of a fixed topology (obtained with $Re = 10$) is also plotted on the figure. For frictional and dynamic pressure drop, the pressure difference across a fixed flow system or channel can be expressed as:

$$P_I - P_O = C_s \,\mathrm{Re}^2 + C_f \,\mathrm{Re}^2 = C\,\mathrm{Re}^2 \qquad (38)$$

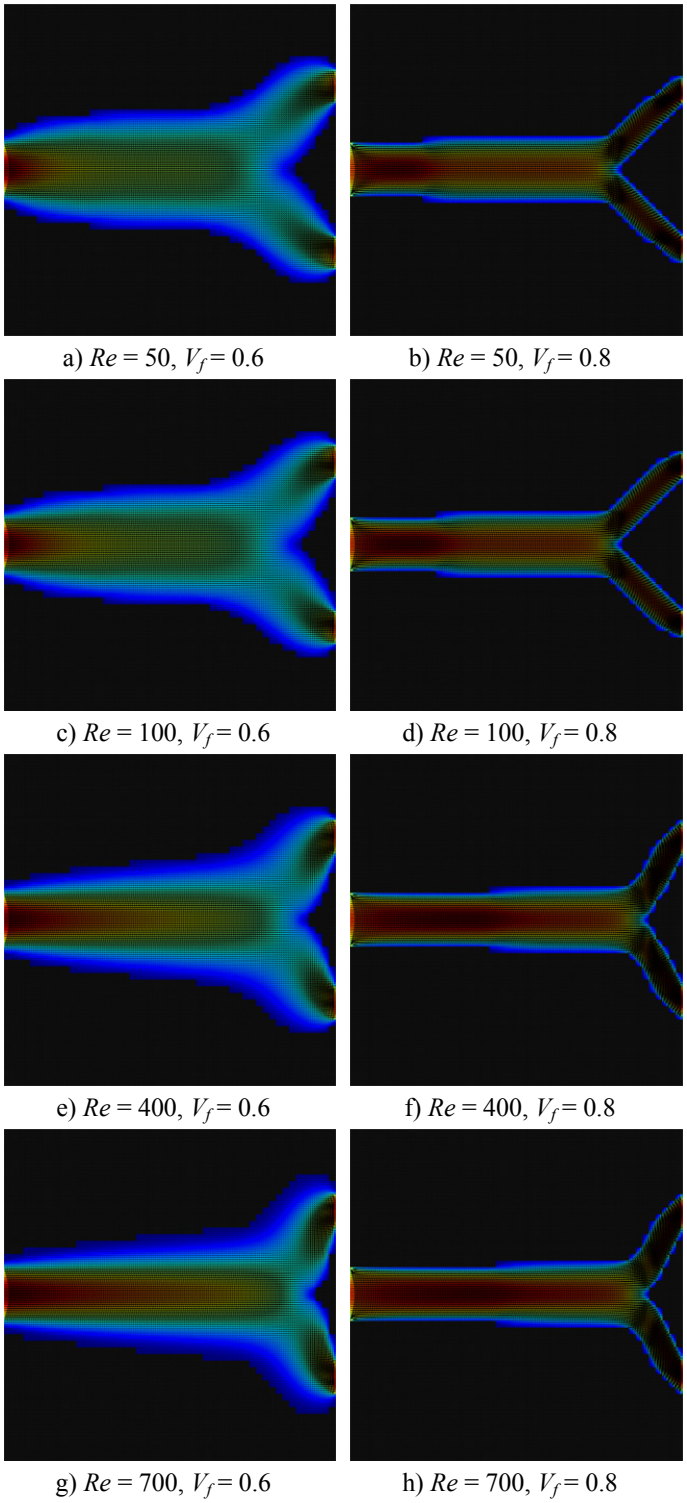

a) $Re = 50$, $V_f = 0.6$ b) $Re = 50$, $V_f = 0.8$

c) $Re = 100$, $V_f = 0.6$ d) $Re = 100$, $V_f = 0.8$

e) $Re = 400$, $V_f = 0.6$ f) $Re = 400$, $V_f = 0.8$

g) $Re = 700$, $V_f = 0.6$ h) $Re = 700$, $V_f = 0.8$

Figure 11 Velocity contours for the one inlet two outlet layout

where C_s is the pressure loss coefficient relating to the change in form or shape, C_f is the pressure loss coefficient to due friction and C is the combined or effective pressure loss coefficient.

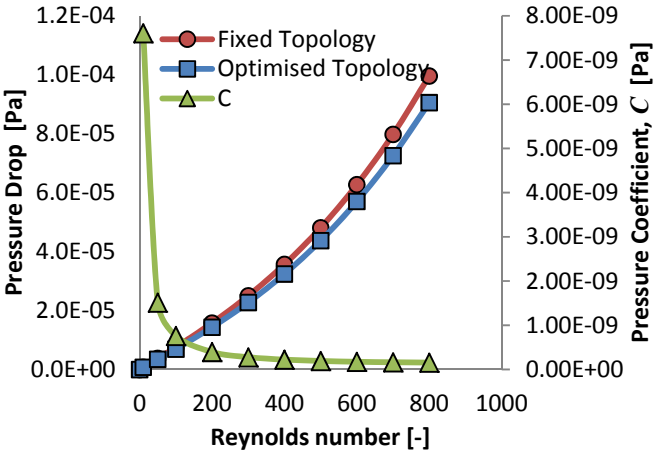

Figure 12 Pressure drop for optimal layout at $V_f = 0.8$

This follows from the base relationship between the pressure drop and velocity squared for a constant friction factor with dynamically similar configurations. The effective pressure loss coefficient is inversely proportional to the Reynolds number squared and remaining approximately constant for high Reynolds numbers ($Re > 400$).

$$C \propto \frac{1}{\mathrm{Re}^2} \tag{39}$$

The influence of varying friction factor, which scales linearly in the laminar flow regime was not incorporated when calculating the C values presented in Figure 12. As can also be seen from Figure 12, the topologies that were specifically produced for a particular Reynolds number case outperformed the fixed topological case by approximately 10%. For the $V_f = 0.6$ configurations, the optimized topological cases still outperformed the fixed topological case but the results were less significant. This results in an operating pumping power saving, but requires that the topology be specifically designed for the applicable flow rate requirements.

CONCLUSION

Topology optimization was successfully applied to steady incompressible flow system with the application in for instance flow distribution systems in laminar flow. A square domain divided into 50 by 50 design cells with a further computational sub-cell refinement of 1 by 1, 2 by 2 and 3 by 3 was considered. It was found that when flow channels were wide, the sub-cell refinement strategy did not influence the converged topology or final pressure drop performance of the systems significantly. However, when narrower channels are present such a refinement may be critical. It was also found that the inlet flow rate, expressed in terms of the inlet Reynolds number, had an influence on the obtained topologies, and that the flow-rate-specific topology was important to reduced pumping power requirements. Based on the examples considered in this paper, topology optimization is a useful tool for designing efficient flow systems.

FURTHER WORK

Temperature based objective functions and weighted multi objective function that include both thermal and flow dissipation principles are to be considered, especially for cooling applications

REFERENCES

[1] Bruns T, Tortorelli D., "Topology optimization of non-linear elastic structures and compliant mechanisms", Computer Methods in Applied Mechanics and Engineering, 190, 26-27, pp 3443–3459, 2001

[2] Gersbor-Hansen A, Sigmund O, Haber RB, "Topology optimization of channel flow problems", Struct. Multidisc. Optim., 29, pp 1-12, 2005

[3] Borvall T, Petersson J, "Topology optimization of fluids in stokes flow", Int J Numer Methods Fluids, 41, pp 77-107, 2003

[4] Othmer C, "A continuous adjoint formulation for the computation of topological and surface sensitivities of ducted flows", Int. J. Numer. Meth. Fluids, 58(8),861–877, 2008.

[5] Bendsøe MP, Kikuchi N, "Generating optimal topologies in structural design using a homogenization method.", Comput Methods Appl Mech Eng, 71, pp. 197-224, 1988

[6] Bendsø MP, Sigmund O., "Material interpolation schemes in topology optimization", Archive of Applied Mechanics 1999;69(9):635–654.

[7] Bendsøe MP, Sigmund O, "Topology optimization: theory, methods and applications", Springer Verlag, 2nd Edtition, 2003, ISBN 3540429921

[8] Gersbor-Hanse A, Bendsøe MP, Sigmund O, "Topology optimization of heat conduction problems using the finite volume method", Struct. Multidisc. Optim, 30, pp 251-259, 2006

[9] Donoso A, Sigmund O. Topology optimization of multiple physics problems modelled by Poissons equation. *Latin American Journal of Solids and Structures* 2004;**1**:169–184.

[10] Nadarajah S, Jameson A., "A comparison of the continuous and discrete adjoint approach to automatic aerodynamic optimization.", , AIAA 38th Aerospace Sciences Meeting and Exhibit, AIAA paper 2000-0667, Reno, NV, January 2000.

[11] Nadarajah S, Jameson A. "Studies of the continuous and discrete adjoint approaches to viscous automatic aerodynamic optimization", AIAA 15th Computational Fluid Dynamics Conference, AIAA paper 2001-2530, Anaheim, CA, June 2001.